Phase Sensitive X-Ray Diffraction Imaging of Defects in Biological Macromolecular Crystals

Z. W. Hu,[1,*] B. Lai,[2] Y. S. Chu,[2] Z. Cai,[2] D. C. Mancini,[2] B. R. Thomas,[1,3] and A. A. Chernov[1]

[1]*Universities Space Research Association, NASA/Marshall Space Flight Center, Huntsville, Alabama 35812*

[2]*Advanced Photon Source, Argonne National Laboratory, Argonne, Illinois 60439*

[3]*Center for Microgravity Materials Research, University of Alabama in Huntsville, Huntsville, Alabama 35899*

(Received 7 February 2001; published 12 September 2001)

Conventional x-ray diffraction topography is currently used to map defects in the bulk of protein crystals, but the lack of sufficient contrast is frequently a limiting factor. We experimentally demonstrate that this barrier can be circumvented using a method that combines phase sensitive and diffraction imaging principles. Details of defects revealed in tetragonal lysozyme and cubic ferritin crystals are presented and discussed. The approach enabling the detection of the phase changes of diffracted x rays should prove to be useful in the study of defect structures in a broad range of biological macromolecular crystals.

DOI: 10.1103/PhysRevLett.87.148101 PACS numbers: 87.59.–e, 41.60.Ap, 61.72.Ff, 87.14.Ee

The substantial decrease in source size and source divergence offered by advanced synchrotron x-ray sources has led to an upsurge in developing various types of coherence-based x-ray imaging and diffraction techniques [1–8]. Refraction-based phase contrast x-ray imaging [8] among others benefits greatly from the unique property of spatial coherence possessed by third generation sources [4], and holds promise for biological and medical applications from the capability to distinguish regions of slightly differing refractive indexes where absorption contrast is weak or even undetectable. By invoking a highly coherent hard x-ray beam, spectacular diffraction-based phase contrast effects have been observed in diffraction images [6].

Conventional x-ray topographs are maps of the diffracted beam intensity of a crystal [9]. Any potential interaction or interference between different rays of the diffracted beam that may occur outside the exit boundary of the crystal is usually ignored within the scope of classical x-ray topography. Yet the difference in x-ray scattering power and wave propagation between a lattice faulted area and the near-perfect bulk of a small molecule crystal is normally large enough to give rise to appreciable diffraction contrast of defects in conventional topographs. However, this may not be often the case in dealing with dislocations and other microdefects in macromolecular crystals where the x-ray scattering strength is extremely weak [9,10]. Uniformly grown macromolecular crystals, e.g., lysozyme [11,12], tomato bushy stunt virus [13], often appear dislocation-free (superficially better than Si) in conventional x-ray topographs while, in reality, they may contain defects [14], or could be rather poorly ordered in terms of diffraction performance [13]. As was the case with semiconductors before the 1950's [15], the role of defects as essential entities in the bulk of macromolecular crystals remains unclear, as a whole, largely because of the lack of new methods that allow dislocations and other lattice irregularities to be detected and characterized with sufficient sensitivity, though defects on crystal surfaces can be observed during growth, for example, by using atomic force microscopy [16–18] or by *in situ* etching [14].

In this Letter, we employ a phase sensitive x-ray diffraction imaging approach for augmenting the contrast of defects in protein crystals. The variety of defects has been observed in great detail, for the first time, by enhanced contrast in the bulk crystals of a hen egg-white lysozyme (HEWL) (a small protein with a roughly ellipsoidal shape and dimensions $30 \times 30 \times 50$ Å) and ferritin (a large spherical protein with an external diameter 120–130 Å). The work demonstrates that the coherence-based imaging method is extremely sensitive to lattice irregularities. It should provide a new way to characterize structural defects, their properties, and the causes of lattice disorder effectively in a wide spectrum of macromolecular crystal systems.

Experiments were carried out at 2BM of SRICAT, Advanced Photon Source (APS). A Si(111) double-bounce monochromator was used to deliver an approximately monochromatic beam with an angular divergence of 2×10^{-5} rad and the beam pass, $\Delta\lambda/\lambda$, $\sim 1.48 \times 10^{-4}$ at a wavelength of 0.96 Å. The transverse coherence lengths are ~ 66 μm vertically and ~ 16 μm horizontally. Thus, crystal defects are properly sized microstructural objects for examination in terms of the spatial coherence. Note that the requirement for the longitudinal coherence can be quite relaxed for phase imaging [19,20]. A six-circle Huber diffractometer was employed along with a scintillation detector and a charge-coupled device (CCD) camera to perform rocking-curve and imaging measurements (Fig. 1). Well-faceted and optically defect-free tetragonal HEWL and cubic ferritin crystals grown by a batch method [21] were loaded into quartz capillaries for measurements.

Sets of the high-angular-sensitivity x-ray diffraction images of a HEWL crystal are shown in Figs. 2(a)–2(e), taken with mode 2 (Fig. 1) and the reflection of 4 4 0 [Fig. 2(c)]. The images are negatives, i.e., white regions diffract strongly and vice versa. Figures 2(a) and 2(d) were taken at the same angular position on peak M and with the camera placed ~ 7 and 25 cm away from the sample, respectively. A number of defects, such as the dislocations D and L, are discernible in Fig. 2(a). Attention is drawn

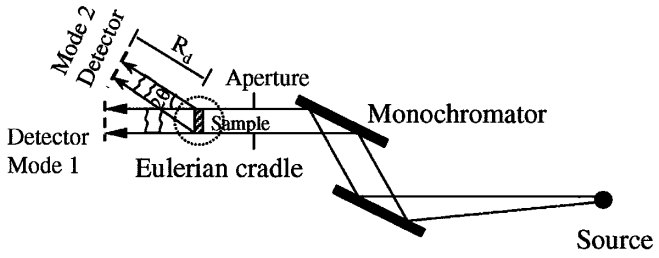

FIG. 1. Schematic drawing of the experimental setup for the phase sensitive diffraction imaging (mode 2), where the diffracted x rays are invoked, and for the phase sensitive radiographic imaging (mode 1) in which the incident x rays are used. The sample-to-source distance, R_s, is ~50 m; the source size, s, is $\sim 145 \times 36$ μm.

to the intensity variation in the strongly diffracted regions with an increase in the sample-to-camera distance, R_d. The dislocations D, the dislocation loops (or half loops) L, and additional structural features in great detail are more clearly visible in Fig. 2(d) than in Fig. 2(a). The substantial defect contrast obtained by properly increasing R_d or defocus [22] (in a way similar to that used for performing the "in-line" phase contrast radiographic imaging [4,19]) is primarily phase contrast. Of course, the resulting imaging patterns of defects are complex in some cases, partly because orientation contrast and the dynamical diffraction effects can come into play as well. A number of linear features originate from the growth sector boundary (GB) at the top-right corner, as observed in solution grown conventional crystals [23]. The middle crystal part, marked M in Fig. 2(d), appears to be less ordered than the near regions. The white regions [Figs. 2(a) and 2(d)] are out of diffraction when the crystal is rocked to the subpeak which is separated from the main peak by 0.005°; a small crystal part [Fig. 2(e)] diffracts strongly instead. A number of defects, marked D in Fig. 2(e), emerge from the center of the crystal and presumably originate from the initial nucleus. The segments of the dislocations in Figs. 2(d) and 2(e) are largely along the ⟨001⟩ and ⟨110⟩ directions, and yet the subtle osmotic pressure [24] might play a role in the dislocation configuration given the intrinsic nature of weak macromolecular bonding. The looplike dislocations are attributed to stress/strain relief around stress centers, e.g., caused by the nonuniform trapping of impurities [25]. Such a center appears discernible in Fig. 2(b).

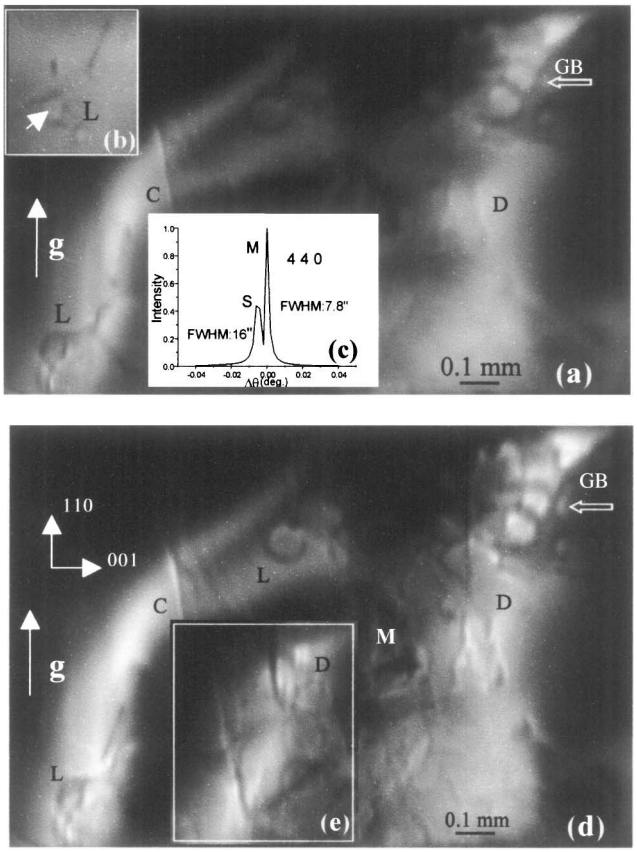

FIG. 2. Phase sensitive diffraction images of a lysozyme crystal taken at the sample-to-detector distance R_d: (a),(b) 7 cm, (d),(e) 25 cm. A black spot marked by an arrow in (b) appears in the center of the loop L. g represents the diffraction vector, GB represents the growth sector boundary, and C represents the microcracks. [(c) see text.]

Figures 3(a) and 3(b) show two diffraction images of a uniformly grown octahedron-shaped ferritin crystal, taken at the same angular position on a rocking curve at $2\theta_B$ corresponding to 4 4 4, but with $R_d \sim 9$ and ~21 cm, respectively. Rich contrast structures are observed more clearly in Fig. 3(b) than in Fig. 3(a). Sets of fine fringes such as those marked $F1$ and $F2$ in Fig. 3(b), along with other strong contrast features, occur abundantly at about the middle of the crystal. A V-shaped interference fringe pattern emerges in an outer growth region, i.e., the upper part of Fig. 3(b), and mimics somewhat the shape of that part of the crystal, although the coarse fringes bend slightly toward the center, as a result of the disturbance of the long-range strains, and coalesce with fine fringes at a planar defect or dislocation bundle (marked P). Two black-white lines crossed at the bottom-left side are the images of the boundaries of mother liquor around the sample, as verified in Fig. 3(d), a phase sensitive radiograph recorded using mode 1. The fringe patterns almost disappear when the crystal is slightly rocked [Fig. 3(c)]. Another set of fine fringes (marked $F3$) is shown in Fig. 3(e), where only a small crystal part diffracts. The upper part of Fig. 3(b) turns out to be nearly defect-free when the crystal is oriented such that the V-shaped fringe pattern disappears [Fig. 3(f)].

The dynamical diffraction effects [26] from the lysozyme crystal are expected to be less significant in terms of the ratio of the crystal thickness ~0.3 mm to the 4 4 0 extinction length ~2 mm. This may be true also in the ferritin crystal case provided that the extinction distance of the reflection used is ~6.5 mm, in comparison with the sample thickness varying from 0.1 to 0.7 mm. In our cases, a defect (object) can be considered as a perturbation source which modifies the wave front of a part of the outgoing beam diffracted at the defective region. When this modified part (the object wave) interacts with an unperturbed

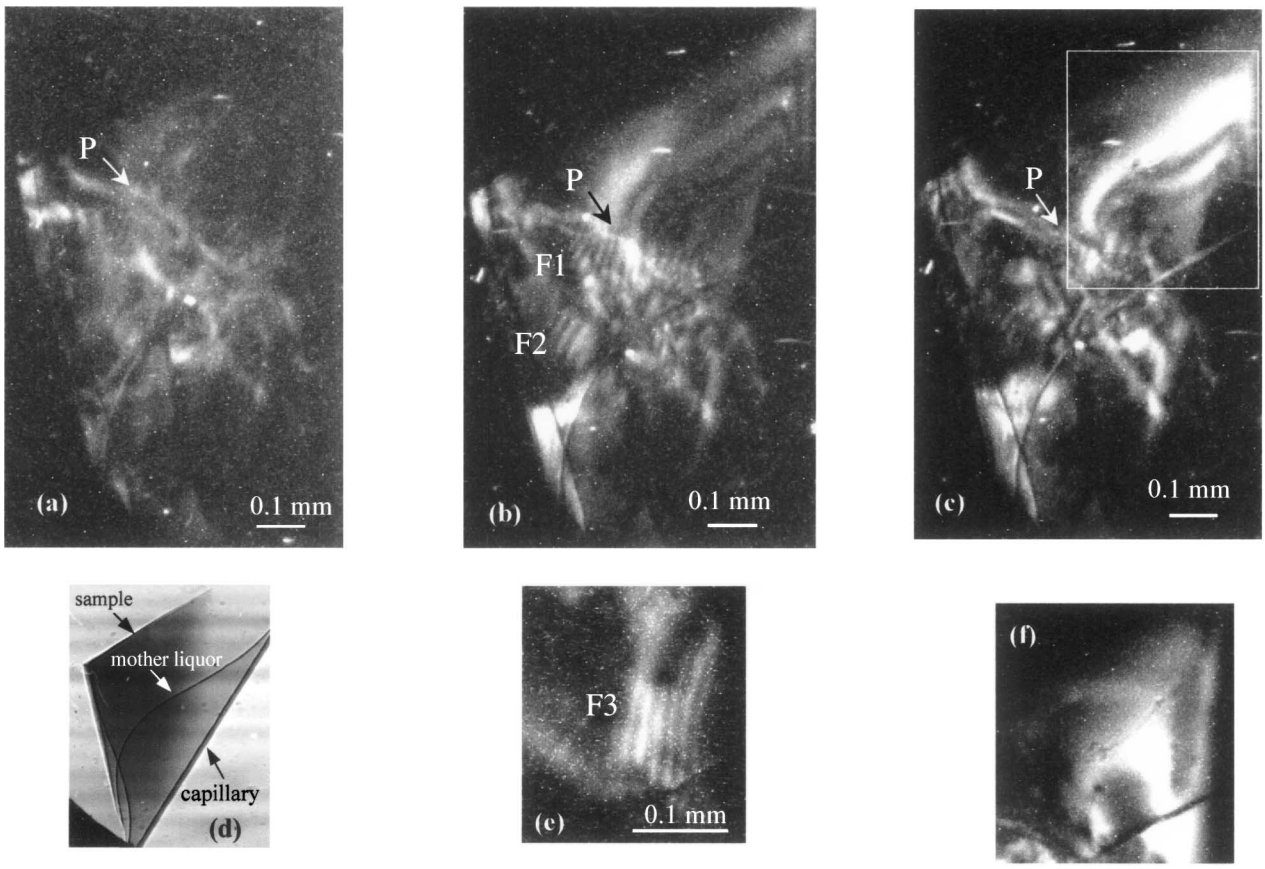

FIG. 3. Phase sensitive diffraction images of a ferritin crystal taken at the sample-to-detector distance R_d: (a) 9 cm, (b) 21 cm, (c) 21 cm [(c) was taken by changing $\Delta\theta \sim -0.001°$ relative to the angle of (b)], (d) phase sensitive radiograph, and (e),(f) taken by varying $\Delta\theta \sim 0.009°$ and $\sim 0.002°$ with respect to the angle in (b), respectively. Panel (f) corresponds to the delineated crystal area in (c); a slight lattice bending is observed.

part (the reference wave that provides a basis from which the phase changes can be measured) diffracted from the surrounding "near-perfect" region, interference can be yielded. This primarily accounts for the enhanced contrast effects. From the context, the wave field responsible for the imaging pattern of the defect may be written by

$$D(\mathbf{r}) = \exp(-2\pi i \mathbf{k}_g \cdot \mathbf{r}) + c \int \frac{\exp(-2\pi i k_{g'} |\mathbf{r} - \mathbf{r}'|}{|\mathbf{r} - \mathbf{r}'|} \times \varphi(\mathbf{r}') \exp(-2\pi i \mathbf{k}_g \cdot \mathbf{r}') \, d\mathbf{r}', \quad (1)$$

where $\varphi(\mathbf{r}')$ is the perturbation potential in the effective size of the defect, c is a constant, and $\mathbf{k}_g$ and $\mathbf{k}_{g'}$ denote the wave vectors of the unperturbed and perturbed diffracted waves, respectively. The individual defect imaging pattern resembles a Fresnel hologram in general [27]. If the camera is placed in the far field of the defect (but not necessarily in the far field of the whole sample), the intensity distribution may follow

$$I = 1 + \frac{2c}{R_d} \left\{ \cos\left[\frac{\pi(x^2 + y^2)}{\lambda R_d}\right] \mathrm{Re}F(\mathbf{q}) + \sin\left[\frac{\pi(x^2 + y^2)}{\lambda R_d}\right] \mathrm{Im}F(\mathbf{q}) \right\} + \frac{c^2}{R_d^2} |F(\mathbf{q})|^2. \quad (2)$$

Then, the scattering amplitude $F(\mathbf{q}) = \int \varphi(\mathbf{r}') \times \exp(2\pi i \mathbf{q} \cdot \mathbf{r}') \, d\mathbf{r}'$, where $|\mathbf{q}| = |\mathbf{k}_{g'} - \mathbf{k}_g|$ (the transverse spatial frequency). The middle term in Eq. (2) is a dominant one, and refers to the interference between the diffraction pattern of the defect and the coherent reference wave. For a line or point defect with a radius (R), say, 1 μm, then $(R)^2/\lambda = 10$ mm for $\lambda = 1$ Å. Thus, the Fraunhofer diffraction hologramlike imaging effects would be practically obtainable. The fringe patterns [$F1$ and $F2$ in Fig. 3(b), and $F3$ in Fig. 3(e)] can be interpreted as the interference effects of overlapping waves arising largely from small lattice rotations. Then, the angle of the overlapping x-ray waves is about 5×10^{-6} rad for the $F1$ pattern, 4×10^{-6} rad for $F2$, and 7×10^{-6} rad for the $F3$ fringes based on the measured spacings of the fringes. The small lattice rotations, 10^{-5} to 10^{-6} rad, would be hardly detectable with orientation contrast. With this model, the fringes of this type (formed in different crystal areas by rocking the crystal) can be readily explained. The V-shaped fringe system shown in Fig. 3(b) appears to be of *Pendellösung* fringes given the "wedge-shaped" crystal. On the other hand, the fringe system resembles the interference effects from the phase-correlated facet edges which form a type of composite "Fresnel's biprism" [28,29]. Further work is underway.

This Letter demonstrates that lattice defects and irregularities in weakly scattering protein crystals can be thoroughly mapped by simply incorporating phase information of exit x-ray waves into diffraction imaging. The direct mapping of the distribution of defects and the variation of the intrinsic structural quality across the whole crystal would provide insights into macromolecular crystal perfection and growth, and have an impact on structural biology as well. The intensity distribution of defect images and the strength of interference effects obtained by this method correlate directly with the nature and types of defects and how well the lattices are defined, as well as the degree of coherence of the incident x-ray beam. Therefore, this imaging approach potentially allows both physical defects in great detail and correlation of molecules in position in the crystals to be evaluated in terms of varying contrast throughout the crystals. Applying this approach to various types of biological macromolecular systems would enable detailed investigation of defects and their formation in relation to growth conditions and postcrystallization.

Z. W. H. wishes to thank Dr. Francesco De Carlo for his help with the initial setting up of the CCD camera, and Professor Liqing Chen for his help with examination of structure factors. This research was supported by NASA (under NCC8-66-050 and an ITD award). Use of the APS was supported by DOE, BES, Office of Science, under W-31-109-Eng-38.

*Email address: zhengwei.hu@msfc.nasa.gov

[1] M. Howells *et al.,* Science **238**, 514 (1987).
[2] M. Sutton *et al.,* Nature (London) **352**, 608 (1991).
[3] W. B. Yun, P. J. Viccaro, B. Lai, and J. Chrzas, Rev. Sci. Instrum. **63**, 582 (1992).
[4] A. Snigirev, I. Snigireva, V. Kohn, S. Kuznetsov, and I. Schelokov, Rev. Sci. Instrum. **66**, 5486 (1995).
[5] I. K. Robinson *et al.,* Phys. Rev. B **52**, 9917 (1995).
[6] Z. W. Hu, P. A. Thomas, A. Snigirev, I. Snigireva, A. Souvorov, P. G. R. Smith, G. W. Ross, and S. Teat, Nature (London) **392**, 690 (1997).
[7] J. Miao, P. Charalambous, J. Kirz, and D. Sayre, Nature (London) **400**, 342 (1999).
[8] R. Fitzgerald, Phys. Today **53**, 23 (2000), and references therein.
[9] D. K. Bowen and B. K. Tanner, *High Resolution X-Ray Diffractometry and Topography* (Taylor & Francis, London, 1998).
[10] The weak scattering strength, or rather the weak scattering power, means a large extinction length ξ_g. The minimum crystal thickness required for formation of the direct image of defects is $\sim 0.3\xi_g$. For macromolecular crystals, the extinction distance at radiation 1 Å could reach tens of millimeters even for strong reflections. As a result, only mosaic blocks and those defects where an effective misorientation is larger than the divergence of incident x rays are observable in conventional topographs whereas dislocations and other microdefects are less likely to be detected. For small-protein crystals, the contrast of dislocations may be resolved in extremely thick samples [K. Izumi *et al.,* J. Cryst. Growth **206**, 155 (1999)].
[11] I. Dobrianov, K. D. Finkelstein, S. G. Lemay, and R. E. Thorne, Acta Crystallogr. D **54**, 922 (1998).
[12] F. Otalora, J. M. Garcia-Ruiz, J. A. Gavira, and B. Capelle, J. Cryst. Growth **196**, 546 (1999).
[13] B. Lorber *et al.,* J. Cryst. Growth **204**, 357 (1999).
[14] F. Rosenberger, P. G. Vekilov, M. Muschol, and B. R. Thomas, J. Cryst. Growth **168**, 1 (1996).
[15] H. J. Queisser and E. E. Haller, Science **281**, 945 (1998).
[16] A. McPherson, *Crystallization of Biological Macromolecules* (Cold Spring Harbor Laboratory Press, New York, 1998).
[17] T. A. Land, J. Malkin, Y. G. Kuznetsov, A. McPherson, and J. J. DeYoreo, Phys. Rev. Lett. **75**, 2774 (1995).
[18] S. T. Yau, B. R. Thomas, and P. G. Vekilov, Phys. Rev. Lett. **85**, 353 (2001).
[19] S. W. Wilkins *et al.,* Nature (London) **384**, 335 (1996).
[20] G. Margaritondo and G. Tromba, J. Appl. Phys. **85**, 3406 (1999).
[21] B. R. Thomas, D. Carter, and F. Rosenberger, J. Cryst. Growth **187**, 499 (1998).
[22] J. M. Cowley, *Diffraction Physics* (North-Holland, Amsterdam, 1995), 3rd revised ed.
[23] S. Ikeno, H. Maruyama, and N. Kato, J. Cryst. Growth **3-3**, 683 (1968).
[24] D. E. McRee, *Practical Protein Crystallography* (Academic Press, San Diego, 1999), 2nd ed.
[25] A. A. Chernov, *Modern Crystallography III: Growth of Crystals* (Springer, Berlin, 1984).
[26] B. W. Batterman and H. Cole, Rev. Mod. Phys. **36**, 681 (1964).
[27] S. Kuznetsov *et al.,* Phys. Status Solidi (a) **172**, 3 (1999).
[28] M. Born and E. Wolf, *Principles of Optics* (Cambridge University Press, Cambridge, 1999), 7th ed.
[29] A. R. Lang and A. P. W. Makepeace, J. Phys. D **32**, A172 (1999).